

# Investigation of internal intermittency by way of higher-order spectral moments

S. Lortie<sup>1</sup> and L. Mydlarski<sup>1,†</sup>

<sup>1</sup>Department of Mechanical Engineering, McGill University, 817 Sherbrooke Street West, Montréal, QC, H3A 0C3, Canada

(Received 7 May 2021; revised 17 October 2021; accepted 21 October 2021)

The analysis of turbulence by way of higher-order spectral moments is uncommon, despite the relatively frequent use of such statistical analyses in other fields of physics and engineering. In this work, higher-order spectral moments are used to investigate the internal intermittency of the turbulent velocity and passive-scalar (temperature) fields. This study first introduces the theory behind higher-order spectral moments as they pertain to the field of turbulence. Then, a short-time Fourier-transform-based method is developed to estimate these higher-order spectral moments and provide a relative, scale-by-scale measure of intermittency. Experimental data are subsequently analysed and consist of measurements of homogeneous, isotropic, high-Reynolds-number, passive and active grid turbulence over the Reynolds-number range  $35 \leq R_\lambda \leq 731$ . Emphasis is placed on third- and fourth-order spectral moments using the definitions formalised by Antoni (*Mech. Syst. Signal Pr.*, vol. 20 (2), 2006, pp. 282–307), as such statistics are sensitive to transients and provide insight into deviations from Gaussian behaviour in grid turbulence. The higher-order spectral moments are also used to investigate the Reynolds (Péclet) number dependence of the internal intermittency of velocity and passive-scalar fields. The results demonstrate that the evolution of higher-order spectral moments with Reynolds number is strongly dependent on wavenumber. Finally, the relative levels of internal intermittency of the velocity and passive-scalar fields are compared and a higher level of internal intermittency in the inertial subrange of the scalar field is consistently observed, whereas a similar level of internal intermittency is observed for the velocity and passive-scalar fields for the high-Reynolds-number cases as the Kolmogorov length scale is approached.

**Key words:** intermittency, isotropic turbulence, turbulent mixing

## 1. Introduction

The work of Kolmogorov (1941*a,b*) (referred to herein as K41) proposed the existence of an inertial subrange that separates the dissipative scales from the energy-containing ones

† Email address for correspondence: [laurent.mydlarski@mcgill.ca](mailto:laurent.mydlarski@mcgill.ca)

in the limit of sufficiently high Reynolds numbers. These notions were later extended to passive-scalar fields by Oboukhov (1949) and Corrsin (1951) (referred to herein as KOC), who proposed analogous concepts to those in K41, such as local isotropy of passive-scalar fields and the existence of an inertial–convective subrange. As established by K41 and KOC, two important parameters of turbulent flows are the dissipation rates of the turbulent kinetic energy and scalar variance, respectively defined as

$$\langle \epsilon \rangle = 2\nu \langle s_{ij}s_{ij} \rangle, \tag{1.1}$$

and

$$\langle \epsilon_\theta \rangle = \gamma \left\langle \frac{\partial \theta}{\partial x_i} \frac{\partial \theta}{\partial x_i} \right\rangle, \tag{1.2}$$

where  $s_{ij} = \frac{1}{2}(\partial u_i/\partial x_j + \partial u_j/\partial x_i)$  is the fluctuating strain rate,  $u_i$  is the velocity fluctuation,  $\theta$  is the passive-scalar fluctuation,  $\nu$  is the kinematic viscosity and  $\gamma$  is the scalar diffusivity. K41 and KOC theories make use of the mean dissipation rates ( $\langle \epsilon \rangle$  and  $\langle \epsilon_\theta \rangle$ ). However, it is now known that  $\epsilon$  and  $\epsilon_\theta$  exhibit strong variations in time and space (Landau 1944; Sreenivasan & Antonia 1997; Warhaft 2000) – a phenomenon known as internal intermittency.

The effect of internal intermittency on the predictions of K41 and KOC theories has frequently been described in the context of structure functions. Using the longitudinal velocity ( $u$ ) field as an example, Kolmogorov theory predicts that the  $n$ th-order, inertial-range structure function scaling exponents ( $\zeta_n$ ), defined by

$$\langle [\Delta u(r)]^n \rangle \equiv \langle [u(x+r) - u(x)]^n \rangle \sim r^{\zeta_n}, \tag{1.3}$$

where  $r$  lies within the inertial range, must be equal to  $n/3$ , in the limit of high Reynolds numbers. However, the effects of internal intermittency have been found to change the higher-order scaling exponents, such that (i)  $\zeta_n < n/3$  for  $n > 3$ , and (ii) the deviation from the Kolmogorov prediction increases with increasing structure function order (e.g. Anselmet *et al.* 1984). As a consequence of Kolmogorov’s 4/5 law (or, equivalently, Yaglom’s 4/3 law for passive scalars; Yaglom 1949), the scaling of third-order structure functions must be equal to 1 (their K41/KOC predicted value) and is not affected by internal intermittency. Moreover, the deviation of second-order structure function scaling exponents from their Kolmogorov predictions are theorised to be of the opposite sign to those of the higher-order structure function scaling exponents (i.e.  $\zeta_2 > 2/3$ , Frisch (1995), p. 139). Note that this corresponds to an inertial-range slope of the power spectrum that is steeper than the K41/KOC prediction of  $-5/3$ , the power spectrum being the analogue in the frequency domain of the second-order structure function. However, given that the effects of internal intermittency become more prominent as the statistical order is increased, the deviations arising from intermittency, when considering second-order statistics, are quite small and generally within the uncertainty of the experiments/simulations, which is why higher-order statistics more readily lend themselves to the study of intermittency.

Batchelor & Townsend (1949) were the first researchers to experimentally demonstrate the intermittency of turbulence, especially present at small scales. They differentiated a time series of velocity up to third order and demonstrated that the signal became increasingly intermittent as the order of differentiation increased, observing periods of activity followed by periods of relative quiescence. They used the flatness factor of the

velocity derivative

$$F_n \equiv \frac{\langle (\partial^n u / \partial x^n)^4 \rangle}{\langle (\partial^n u / \partial x^n)^2 \rangle^2}, \quad (1.4)$$

to quantify the extent to which the probability density function (PDF) of the velocity field deviated from that of a Gaussian distribution and observed a tendency of the flatness factor to increase with the order of differentiation ( $n$ ). Kennedy & Corrsin (1961) subsequently demonstrated that the findings of Batchelor & Townsend (1949) were particular to turbulence by (experimentally and analytically) showing that this increase in flatness factor did not occur for all nonlinear random processes. Further work by Kuo & Corrsin (1971) attempted to locate the intermittency in wavenumber space by band-pass filtering turbulent signals and calculating the flatness factor within each band. They observed that the flatness (and thus the intermittency) increased when increasing the centre frequency of the band. They also found that the flatness tended to 3 at low wavenumbers, implying that the large scales of turbulence exhibited little intermittency. Additionally, they reinforced the idea that the degree of intermittency is Reynolds-number dependent by overlaying their results with those of Batchelor & Townsend (1949) and Wyngaard (1967), showing that the flatness factor (measured over all scales of the turbulence) increased with Reynolds number. Research in more recent years has suggested that the flatness factor of the first derivative of the (longitudinal) velocity fluctuation increases monotonically with Reynolds number, possibly as  $F_1 \sim R_\lambda^{3/8}$  (see Van Atta & Antonia 1980; Sreenivasan & Antonia 1997), although more recent work by Djenidi, Antonia & Tang (2019) claims that the flatness factor reaches a plateau at high Reynolds numbers. The relationship between the flatness factor of derivatives and the Reynolds number has also been described using the multifractal formalism (e.g. Nelkin 1990). The intermittency of passive-scalar fields has been subjected to less scrutiny, although data compiled by Sreenivasan & Antonia (1997) depict a stronger Reynolds-number dependence of the flatness factor of the scalar derivative than that of the longitudinal velocity derivative. Additionally, Sreenivasan & Antonia (1997) point out that the deviations from Gaussian behaviour of passive-scalar fields are typically more significant than those of velocity fields, thus implying a stronger level of intermittency in scalar fields. It has moreover been demonstrated that intermittency in scalar fields can even occur when advected by (non-intermittent) Gaussian velocity fields (Pumir, Shraiman & Siggia 1991; Holzer & Siggia 1994; Kraichnan 1994). Warhaft (2000) also confirmed that the intermittent behaviour of passive-scalar fields extends to scales larger than the dissipative ones, as is the case for velocity fields. Lepore & Mydlarski (2012) used the kurtosis of passive-scalar increments ( $\Delta\theta = [\theta(x+r) - \theta(x)]$ ) to study the evolution of intermittency with separation  $r$  and found that scalar fields exhibited significant departures from the Gaussian predictions for small and intermediate separations. However, it is worth noting that structure functions include contributions from all scales less than or equal to the scale  $r$  over which the increments are calculated (Meyer, Mydlarski & Danaïla 2018).

Although our understanding of internal intermittency has greatly improved with time, questions remain. For example, the scale dependence of internal intermittency within velocity and/or passive-scalar fields has not been extensively studied, even though the spectral nature of turbulent fields has been the object of much research. Spectral-based tools to detect bursts and transients have been used extensively in other fields of physics and engineering, especially in fault detection of rolling machines and bearings (see Antoni & Randall 2006; Leite *et al.* 2016, and Hu *et al.* 2019). Herein, we use the term ‘transients’ to denote fluctuations that are substantially different (generally non-Gaussian) from those

that are typical of the non-stationary, but statistically steady, flow. Another example is the use of higher- (i.e. third- and fourth-) order spectral moments to analyse acoustic signals contaminated by under-ice noise (Dwyer 1983). Dwyer argued that conventional spectral analysis methods (such as power spectral densities) are incapable of detecting highly impulsive and non-Gaussian transients, and that higher-order spectral moments are more appropriate. He separately used the real and imaginary parts of the complex third- and fourth-order normalised moments (i.e. the spectral skewness and kurtosis) to identify transients of under-ice noise in the frequency domain. Pagnan, Ottonello & Tacconi (1994) later refined the technique and favoured the use of the magnitude of the complex fourth-order moment to obtain a more complete picture of the transients present in the signal. When using this method, however, one must be aware of the change of expected distributions due to the squaring operations necessary to obtain the magnitude of the complex Fourier modes. Antoni (2006) subsequently undertook a more rigorous derivation of the properties of the spectral kurtosis, demonstrating that this higher-order moment is particularly well suited for the detection of transients in a signal. However, he also demonstrated that care must be taken in constructing an appropriate estimation method that favours the detection of short transients. With a few exceptions, such approaches have generally not been applied to turbulent flows, which are nonetheless both spectral and intermittent in nature. Successful attempts at isolating deviations from Gaussian behaviour in wavelet space have been presented by Meneveau (1991) and Farge (1992), although these studies only considered the behaviour of velocity fields (without passive scalars) and limited their analysis to wavelet decomposition, as opposed to the more common Fourier analysis. As discussed in Bos, Liechtenstein & Schneider (2007), there is a clear correspondence between Fourier- and wavelet-based analyses. Although wavelet decompositions can also be used, we favour the use of higher-order moments in the frequency domain for the present work because they constitute a natural extension to the power spectrum (i.e. the second-order spectral moment) while still allowing the flexibility to focus on different ranges of turbulent activity in wavenumber space by varying the size of the analysis window. The use of fourth-order moments in the Fourier domain for the analysis of turbulence was investigated by Chevillard *et al.* (2005), who calculated the flatness factor of experimental velocity data in the frequency domain to demonstrate the higher level of intermittency of vorticity compared with longitudinal velocity.

Given the above, the objective of the present study is threefold. First, we investigate internal intermittency in turbulent flows by way of third- and fourth-order spectral moments. To do so, we propose a short-time Fourier-transform-(STFT-) based method (similar to that of Antoni 2006) that makes use of higher-order spectral moments to quantify the internal intermittency in the frequency/wavenumber domain. The proposed tool (i) does not necessitate band-pass filtering of time series of data, (ii) permits the investigation of internal intermittency as a function of frequency/wavenumber and (iii) allows the possibility of variable window lengths (discussed in later sections), akin to the analysis of Antoni (2006). The second objective is to make use of higher-order spectral moments to explore the Reynolds-number dependence of the internal intermittency of both velocity and scalar fields. Finally, the third objective is to compare the intermittency of both velocity and passive-scalar fields on a spectral basis.

## **2. Theory and implementation of spectral moments**

As noted in § 1, higher-order spectral moments are seldom used in fluid mechanics, although they are encountered much more commonly in other fields of physics and engineering, such as those mentioned above. Similar tools are used herein to detect

intermittent behaviour in turbulent signals caused by internal intermittency. This section begins with a presentation of the mathematical background necessary to calculate higher-order spectral moments. It is followed by a discussion of the method used to analyse time series of turbulent velocity and passive-scalar fields.

### 2.1. Mathematical background

Let a continuous process  $x(t)$  be sampled at a frequency  $f_s$ . The resulting discrete time series can then be divided into  $M$  segments of length  $N$  (via the use of windowing functions, which will be discussed in depth in § 2.2), such that the sampled time series can be denoted as

$$x(n, m) = x([n + N(m - 1)]/f_s), \quad (2.1)$$

with  $n = 0, \dots, N - 1$  and  $m = 1, \dots, M$ . The discrete Fourier transform of each individual segment (denoted by  $m$ ) is then calculated as follows:

$$X(\omega_n, m) = \sum_{k=0}^{N-1} x(k, m) e^{jkn/N}, \quad (2.2)$$

where  $j = \sqrt{-1}$  and  $\omega_n = 2\pi n f_s / N$ . Note that this operation is normally performed using the fast Fourier transform (FFT) algorithm. The power spectral density (referred to as the ‘spectrum’ from here on) is calculated from the average of the square of the modulus of  $X(\omega_n, m)$ , evaluated at each frequency bin (centred at  $\omega_n$ ), over each segment of length  $M$

$$E(\omega_n) = \frac{1}{f_s M} \sum_{m=1}^M |X(\omega_n, m)|^2, \quad (2.3)$$

where the factor  $1/f_s$  is necessary, such that:

$$\langle x^2 \rangle = \int_{-\infty}^{\infty} E(\omega_n) d\omega_n. \quad (2.4)$$

This segmenting and averaging method has multiple advantages, including a reduction in the number of computations required (since it is more efficient to take the FFT of multiple short segments than taking the FFT of the equivalent longer segment) and a lower noise level (Welch 1967).

Although the spectrum is used extensively in the study of turbulence to compare the relative intensity of the fluctuations at the various scales of the turbulence, it fails to capture the non-Gaussian behaviours induced by internal intermittency because it is not very sensitive to the tails of the distribution of a signal (Kuo & Corrsin 1971; Dwyer 1983). The spectrum is therefore not well suited for situating intermittency in wavenumber space. As previously noted, attempts to experimentally filter velocity signals using narrow bands to locate intermittency in wavenumber space have been made (e.g. Kuo & Corrsin 1971), but there exists a simple, flexible (in terms of frequency bin resolution) and rigorous alternative that employs the frequency-domain signal  $X(\omega_n, m)$  to locate and quantify intermittency in the frequency/wavenumber domain. This method makes use of higher-order spectral moments, which are able to capture deviations from Gaussian behaviour in the tails of the PDFs. By viewing the  $N$  segments of data created from the

signal  $x(t)$  as independent observations, one can create a PDF of the spectral coefficients at each frequency bin, and then define the spectral skewness,  $\tilde{S}$

$$\tilde{S}(\omega_n) = \frac{\frac{1}{M} \sum_{m=1}^M |X(\omega_n, m)|^3}{\left(\frac{1}{M} \sum_{m=1}^M |X(\omega_n, m)|^2\right)^{3/2}}, \tag{2.5}$$

and the spectral kurtosis,  $\tilde{K}$

$$\tilde{K}(\omega_n) = \frac{\frac{1}{M} \sum_{m=1}^M |X(\omega_n, m)|^4}{\left(\frac{1}{M} \sum_{m=1}^M |X(\omega_n, m)|^2\right)^2}, \tag{2.6}$$

as the normalised third- and fourth-order moments of the frequency-domain PDFs. Note that (i) tildes denote spectral moments in this work, and (ii) the above definitions differ slightly from those of the spectral skewness and kurtosis presented by Dwyer (1983), which separately employed the real and imaginary parts of the Fourier-transformed signal ( $X^r(\omega_n, m)$  and  $X^i(\omega_n, m)$ , respectively), producing pairs of spectral moments that must be analysed individually. For a stationary Gaussian process, a spectral skewness of 0 and a spectral kurtosis of 3 are to be expected with Dwyer’s method. However, the aforementioned revised definitions of  $\tilde{S}(\omega_n)$  and  $\tilde{K}(\omega_n)$ , given by Pagnan *et al.* (1994) and Antoni (2006), employ the modulus of the Fourier transform ((2.5) and (2.6)), to simplify each spectral moment to a single parameter. Use of the magnitude of the complex, Fourier-transformed variables changes the nature of their distribution such that Gaussian statistics would give rise to a chi distribution, with the following probability density function (Forbes *et al.* 2011):

$$f(X, \sigma, L) = \frac{2^{1-L/2} X^{L-1}}{\Gamma(L/2) \sigma^L} e^{-X^2/2\sigma^2}, \tag{2.7}$$

where  $L$  is the degree of freedom ( $L = 2$  for the magnitude of complex numbers),  $\sigma$  is the standard deviation of  $X^r(k, l)$  and  $X^i(k, l)$ , and  $\Gamma$  is the gamma function. (See Millioz, Huillery & Martin (2006) for more details.) The raw moments of the chi distribution can thus be calculated from

$$\mu_j = \langle X^j \rangle = \int_{-\infty}^{\infty} X^j \frac{2^{1-L/2} X^{L-1}}{\Gamma(L/2) \sigma^L} e^{-X^2/2\sigma^2} dX, \tag{2.8}$$

which reduces to

$$\mu_j = \sigma^j 2^{j/2} \frac{\Gamma(\frac{1}{2}(L + j))}{\Gamma(\frac{1}{2}L)} \tag{2.9}$$

(Forbes *et al.* 2011). Therefore, if the signal  $x(t)$  is stationary and Gaussian, the definitions proposed in (2.5) and (2.6) lead to a spectral skewness of

$$\tilde{S} = \frac{\mu_3}{\mu_2^{3/2}} = \Gamma(5/2) \approx 1.33, \tag{2.10}$$

and a spectral kurtosis of

$$\tilde{K} = \frac{\mu_4}{\mu_2^2} = 2. \quad (2.11)$$

The present work employs the modulus in the definition of higher-order spectral moments because of its simplicity. It should therefore be recalled that, at a given scale, and in the absence of intermittency, the third- and fourth-order spectral moments of a turbulent velocity or scalar field will take on the values of 1.33 and 2, respectively, at that particular scale.

## 2.2. Spectral moment estimation

The higher-order spectral moment estimation method proposed herein makes use of window functions to create multiple sets of data from a time series  $x(t)$ . The creation of segments proposed in (2.1) is equivalent to the application of a square window and therefore results in considerable amounts of spectral leakage due to the non-negligible sidelobes present in the Fourier transform of the square window. The use of a symmetrical window function that gradually decreases to zero at either end, such as the Hann window, is preferable as it reduces spectral leakage (Press *et al.* 2007). In practice, we therefore multiply the signal under investigation by a window function,  $w(k)$ , before the taking the Fourier transform, such that (2.2) becomes

$$X(\omega_n, m) = \sum_{k=0}^{N-1} w(k)x(k, m) e^{jkn/N}. \quad (2.12)$$

This method, often referred to as the STFT, approximates the spectral content of the signal around the time where the window function is centred. Although the time at which a given spectral event occurs may not be of immediate interest in the analysis of internal intermittency, the repeated extraction of spectral content done by taking the STFT at different times in the signal  $x(t)$  creates a distribution in the frequency domain from which one can extract the third- and fourth-order moments. Note that the STFT coincides with the usual Fourier transform when the window is chosen to be very large (i.e. for  $N$  of the order of the size of the entire record).

Despite its ability to extract the spectral content of a signal and identify frequencies at various points in time, the STFT has certain limitations. The results depend (to a certain extent) on the smoothness of the chosen windowing function, although this dependence was not observed to be strong enough to influence the conclusions presented in later sections. A preliminary analysis (not shown) that compared the Blackman, Chebyshev, Gaussian, Hann (used herein) and rectangular windows demonstrated that similar results are obtained when any windowing function is used, apart from the rectangular one. However, substantial research (e.g. Press *et al.* 2007) has shown that the use of rectangular windows leads to significant spectral leakage, which is the main reason it is not used herein. Of the four windowing functions that gave similar results, the Hann window was favoured for the sake of consistency between our manuscript and previous work done on higher-order spectral moments (e.g. Antoni 2006).

The results of the STFT method are also affected by the length of the chosen windows. To illustrate this, consider the turbulent time series of velocity shown in figure 1(a). The largest wavelength (lowest frequency) that the windowing function (dashed line in figure 1) can resolve corresponds to the width of the window itself. Therefore, any frequency lower than the frequency corresponding to the filtering window's length cannot be resolved.

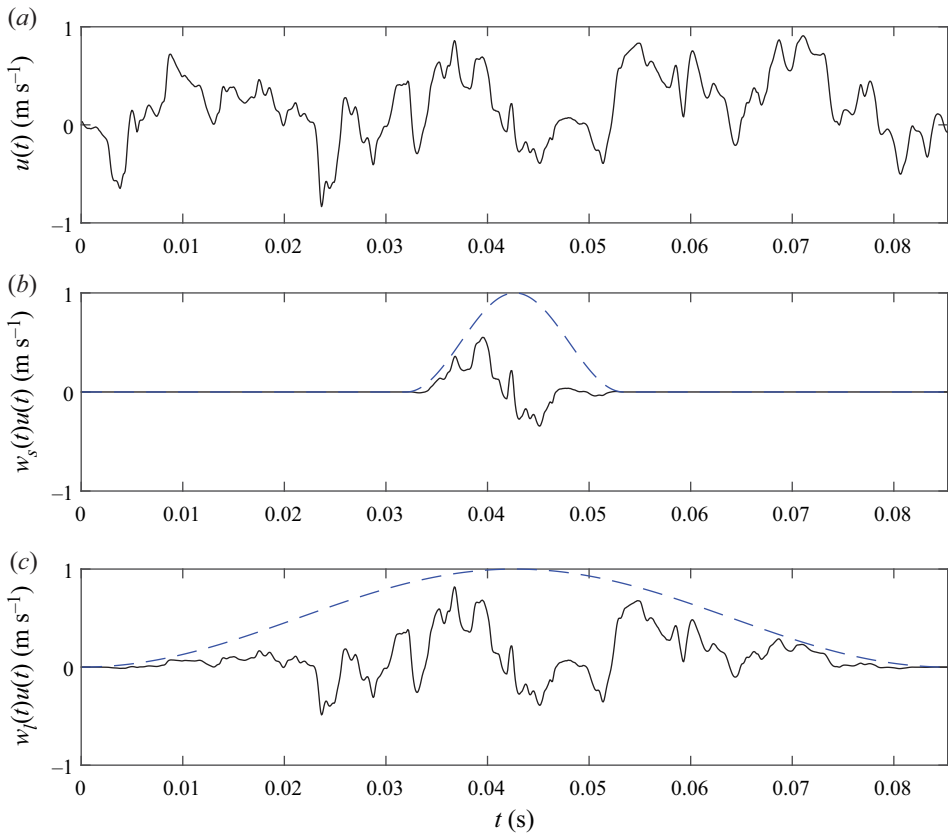


Figure 1. A turbulent velocity time series (—) with window functions (---) applied. (a) The original velocity signal, (b) the velocity signal with a short window applied and (c) the velocity signal with a long window applied.

One solution to this issue is to increase the width of the filtering window (figure 1c). However, as the width of the window increases, issues related to the central limit theorem arise. Specifically, Peligrad & Wu (2010) have demonstrated that, for ergodic processes and for large enough sample sizes, the central limit theorem holds for Fourier transforms. Thus, if a windowed Fourier transform is performed, one should expect the length of the window ( $N$ ) to influence the distribution of the Fourier-transformed data. This is readily demonstrated by considering a hypothetical random variable  $x(t)$  and its sampled time series  $x(n, m)$ . The time series has a skewness of 0.0 and a kurtosis of 2.5, such that its PDF is not Gaussian. A windowed STFT, with window lengths ranging from  $N = 2^2$  to  $N = 2^9$ , was performed on this time series, giving rise to the complex random variable  $X(\omega_n, m)$ . The mean of the kurtosis of this random variable (taken over all frequency bins) was then calculated, first considering only  $X^r(\omega_n, m)$  (i.e. the real part of  $X(\omega_n, m)$ )

$$\langle \tilde{K}^r(\omega_n) \rangle_{\omega_n} = \left\langle \frac{1}{M} \sum_{m=1}^M X^r(\omega_n, m)^4 \right\rangle_{\omega_n} \bigg/ \left( \frac{1}{M} \sum_{m=1}^M X^r(\omega_n, m)^2 \right)^2_{\omega_n}, \quad (2.13)$$



then only  $X^i(\omega_n, m)$  (i.e. the imaginary part of  $X(\omega_n, m)$ )

$$\langle \tilde{K}^i(\omega_n) \rangle_{\omega_n} = \left\langle \frac{1}{M} \sum_{m=1}^M X^i(\omega_n, m)^4 \middle/ \left( \frac{1}{M} \sum_{m=1}^M X^i(\omega_n, m)^2 \right)^2 \right\rangle_{\omega_n} \quad (2.14)$$

and finally  $|X(\omega_n, m)|$  (i.e. the magnitude of  $X(\omega_n, m)$ )

$$\langle \tilde{K}(\omega_n) \rangle_{\omega_n} = \left\langle \frac{1}{M} \sum_{m=1}^M |X(\omega_n, m)|^4 \middle/ \left( \frac{1}{M} \sum_{m=1}^M |X(\omega_n, m)|^2 \right)^2 \right\rangle_{\omega_n}, \quad (2.15)$$

which is simply the mean of the spectral kurtosis defined in (2.6) and noting that  $\langle \cdot \rangle_{\omega_n}$  denotes averaging over all frequency bins. The evolution of these quantities as a function of window length is depicted in figure 2, which depicts how the kurtosis is influenced by the window length. As the window length tends to one ( $N \rightarrow 1$ ), the platykurtic (i.e. sub-Gaussian) character of the original time series forces  $\langle \tilde{K}^r(\omega_n) \rangle$  and  $\langle \tilde{K}^i(\omega_n) \rangle$  to decrease towards the value of the kurtosis of the original time series (2.5). Conversely, as the window length increases toward infinity ( $N \rightarrow \infty$ ),  $\langle \tilde{K}^r(\omega_n) \rangle$  and  $\langle \tilde{K}^i(\omega_n) \rangle$  approach the Gaussian value of 3, even though the original time series  $x(n, m)$  was non-Gaussian. This is a result of the central limit theorem which states that, for a large enough sample size, the distribution of the sample mean (or sample Fourier transform) becomes Gaussian regardless of the original distribution. Note that the behaviour of  $\langle \tilde{K}(\omega_n) \rangle$  is similar, although it does not tend to the value of the kurtosis of the original time series (2.5) as  $N \rightarrow 1$  because of the aforementioned change in distribution resulting from the squaring operation necessary to calculate the magnitude. Moreover, as  $N \rightarrow \infty$ ,  $\langle \tilde{K}(\omega_n) \rangle$  tends to the value of 2 instead of 3, for the reasons discussed in § 2.1.

We have now established that higher-order spectral moments estimated with large windows cannot be used to detect intermittency due to the central limit theorem. Moreover, excessively short windows fail to capture low frequency transients. Therefore, the length of the window used to divide a time series must be chosen with care to ensure that the transient frequencies of interest are captured. If one can estimate the length (or duration) of each transient within the signal, then the window length to be used should correspond to the approximate length of the transient itself. This is attributed to the fact that windows of the same length as, or slightly shorter than, the transients fully encompass these without much interference from the stationary data, which results in strong Fourier modes within the transient frequencies. These strong Fourier modes, which arise from the presence of transients, significantly contribute to the tails of the distributions at the corresponding frequency bins and are more easily captured by higher-order spectral moments. Conversely, the higher-order spectral moments decrease significantly as the window width is increased beyond the length of the transients because the windows that contain the transients become dominated by the stationary data. However, the length of each transient is rarely known *a priori*, and thus the ideal window length to be used remains initially unknown. The solution is therefore to compute the windowed Fourier transform using different window lengths to determine the optimum value (keeping in mind that relatively large windows will systematically result in Gaussian higher-order spectral moments). If one knows the approximate location of the transients in the frequency domain space beforehand, one can identify a few window lengths that may work well. However, in the case where the frequency location of the transients is unknown, one may use the Kurtogram algorithm, proposed by Antoni (2007). This algorithm efficiently conducts

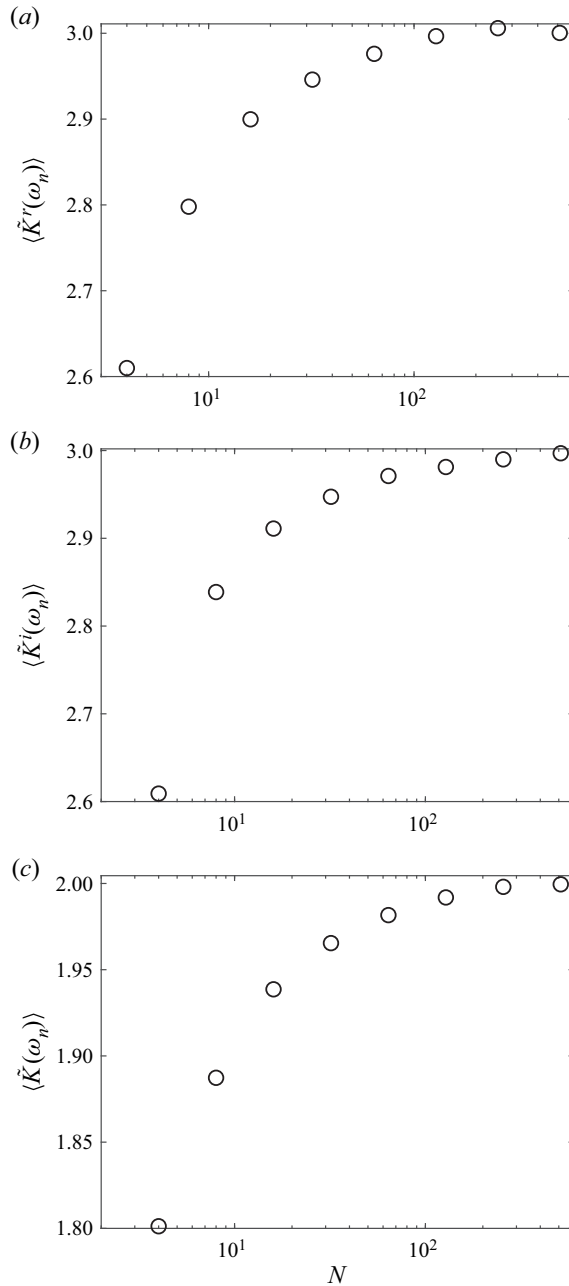


Figure 2. The mean spectral kurtosis plotted as a function of the window length ( $N$ ) expressed in terms of number of samples for (a) the real part of  $X(\omega_n, m)$ , (b) the imaginary part of  $X(\omega_n, m)$  and (c) the magnitude of  $X(\omega_n, m)$ .

a preliminary analysis and sweeps through the signal of interest using multiple window lengths to determine the optimal window to be used for further analysis. The results of this method are analogous to performing successive zooms in wavenumber space. A similar method in which window lengths were increased in successive steps to improve

the frequency resolution was initially used herein to find the approximate locations of the intermittent activity. Then, the most relevant window length to be used for analysis was determined by first establishing the wavenumber range to be studied using higher-order spectral moments (e.g.  $\kappa_{1low} \leq \kappa_1 \leq \kappa_{1high}$ ). The lower bound ( $\kappa_{1low}$ ), which dictated the window size, was selected as a function of the range of scales of interest, whereas  $\kappa_{1high}$  was always equal to  $1/\eta$  in the present work.  $\kappa_{1low}$  was then converted to a frequency (using Taylor's hypothesis:  $f_{low} = \langle U \rangle \kappa_{1low} / (2\pi)$ ), which resulted in the lowest frequency needing to be spanned by the window. The minimum window length (in terms of samples,  $N_{min}$ ) is given by  $N_{min} = f_{samp} / f_{low}$ , where  $f_{samp}$  is the sampling frequency.

### 3. Apparatus

The data analysed herein were obtained by Mydlarski & Warhaft (1998) from experiments conducted in two different wind tunnels in the Sibley School of Mechanical and Aerospace Engineering at Cornell University. The first one has a test section that is  $40.65 \times 40.65 \text{ cm}^2$  in cross-section and 4.5 m long, and the test section of the second one has a  $91.44 \times 91.44 \text{ cm}^2$  cross-section and is 9.1 m in length. The flow parameters for the cases analysed herein are presented in table 1.

For the  $R_\lambda = 35$  and  $R_\lambda = 86$  cases, the turbulence was generated by means of passive grids with 2.54 cm and 10.19 cm mesh lengths, respectively. The turbulent flow fields in all other cases were generated using active grids based on the design of Makita (1991). The active grids contain bars driven by stepper motors that independently actuate rows of agitator wings to create approximately homogeneous, isotropic turbulence (Mydlarski & Warhaft 1996; Mydlarski 2017). Active grids were used in both tunnels to achieve a maximum Taylor microscale Reynolds number of  $R_\lambda = 731$ . A uniform, mean, cross-stream temperature gradient was generated using differentially heated metallic ribbons at the entrance to the wind tunnels' settling chambers. The action of the turbulent velocity field on this mean temperature gradient resulted in a turbulent passive-scalar (temperature) field.

Simultaneous two-component ( $u$ ,  $v$ ) velocity and passive-scalar (temperature) measurements were made in all but two cases. Only longitudinal velocity measurements were made at  $R_\lambda = 671$ , and separate longitudinal velocity and temperature measurements were made  $R_\lambda = 731$ . In these two ( $R_\lambda = 671$  and  $R_\lambda = 731$ ) cases, the velocity measurements were obtained using a single-normal tungsten hot-wire sensor, whereas an X-wire sensor was used for all the other cases. In all cases, hot-wire overheat ratios of 1.8 were employed using Dantec 55M01 constant temperature anemometers. The temperature measurements were made using a cold-wire thermometer sensor placed in a plane parallel to, but 0.5 mm away from, the X-wire sensor. The data were low- and high-pass filtered, and then digitised using an A/D card. Further information on the equipment, as well as detailed descriptions of the wind tunnels and the active grids, are given in Mydlarski & Warhaft (1996) and Mydlarski & Warhaft (1998).

### 4. Results and discussion

Before situating and quantifying internal intermittency in turbulent velocity and scalar fields using the approach outlined in § 2, benchmarking of the algorithm was undertaken to ensure that the algorithm can properly detect transients. Therefore, this section first presents a brief summary of the algorithm's testing procedures and outcomes. This is followed by an investigation of the internal intermittency of turbulent velocity fields by way of higher-order spectral moments. Then, the Reynolds-number dependence of the

Tunnel grid	Horiz. passive	Vert. active	Horiz. passive	Horiz. active	Vert. active	Vert. active	Horiz. active	Vert. active	Horiz. active	Horiz. active	Horiz. active
Mesh (cm)	2.54	5.08	10.2	11.4	5.08	5.08	11.4	5.08	11.4	11.4	11.4
$\langle U \rangle$ (m s <sup>-1</sup> )	6.3	3.3	6.2	3.3	3.6	12.2	3.3	11.4	7	7.3	6.9
$x/M$	70	68	70	62	68	68	62	68	62	35	31
$\beta$ (°C m <sup>-1</sup> )	5.9	4.8	7.4	2.5	3.3	5.2	2.7	3.6	3.6	n/a	5.1
$\nu$ ( $\times 10^6$ m <sup>2</sup> s <sup>-1</sup> )	15.9	16.0	15.8	15.5	16.0	16.0	16.0	16.0	16.0	15.5	15.0
$\langle u^2 \rangle$ (m <sup>2</sup> s <sup>-2</sup> )	0.0134	0.0156	0.0208	0.029	0.0629	0.311	0.0911	1.04	0.583	1.42	1.44
$\langle u^2 \rangle^{1/2} / \langle U \rangle$ (%)	1.8	3.8	2.1	5.2	7.0	4.9	9.1	8.9	10.9	16.4	17.4
$\langle \epsilon \rangle$ (m <sup>2</sup> s <sup>-3</sup> )	0.135	0.0314	0.0559	0.0418	0.118	2.33	0.0833	6.13	0.94	4.48	3.88
$l (= 0.9 \langle u^2 \rangle^{3/2} / \epsilon)$ (m)	0.010	0.056	0.048	0.11	0.12	0.067	0.3	0.16	0.43	0.34	0.4
$R_\lambda (= \langle u^2 \rangle \{15 / (\nu \epsilon)\}^{1/2})$	35	85	86	140	177	197	306	407	582	671	731
$R_l (= \langle u^2 \rangle^{1/2} l / \nu)$	75	440	441	1200	1900	2300	5600	9900	20300	26000	32100
$\eta (= (\nu^3 / \langle \epsilon \rangle)^{1/4})$ (mm)	0.42	0.6	0.52	0.55	0.43	0.21	0.47	0.16	0.26	0.17	0.17
$\langle \epsilon_\theta \rangle$ (°C <sup>2</sup> s <sup>-1</sup> )	0.0284	0.0595	0.140	0.128	0.0665	0.197	0.360	0.215	0.789	n/a	1.70
$\langle \theta^2 \rangle$ (°C <sup>2</sup> )	0.0081	0.062	0.143	0.176	0.083	0.055	0.8	0.08	1.07	n/a	2.05
$l_\theta (= \langle \theta^2 \rangle^{1/2} / \beta)$ (m)	0.015	0.052	0.051	0.17	0.087	0.0451	0.33	0.079	0.29	n/a	0.28
$f_\eta (= \langle U \rangle / (2\pi\eta))$ (kHz)	2.4	0.88	1.9	0.95	1.3	9.4	1.1	11.3	4.3	6.8	6.5

Table 1. Flow parameters. These eleven cases were used to calculate the higher-order spectral moments. The velocity and scalar dissipation rates were determined using  $\langle \epsilon \rangle = 15\nu \int_0^\infty \kappa_1^2 F_{11}(\kappa_1) d\kappa_1$  and  $\langle \epsilon_\theta \rangle = 3\gamma \int_0^\infty \kappa_1^2 F_\theta(\kappa_1) d\kappa_1$ . The Prandtl number ( $Pr$ ) was 0.7.

## Intermittency and higher-order spectral moments

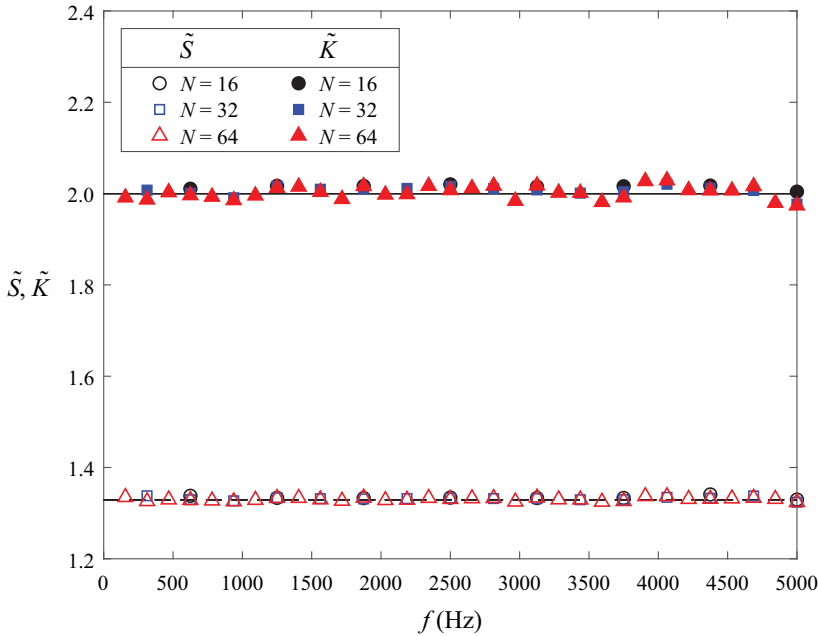


Figure 3. Spectral skewness (open symbols) and kurtosis (closed symbols) of Gaussian white noise evaluated using window lengths of 16 ( $\circ$ ,  $\bullet$  – black), 32 ( $\square$ ,  $\blacksquare$  – blue), 64 ( $\triangle$ ,  $\blacktriangle$  – red) samples. The lines represent the expected values of spectral skewness (dashed) and spectral kurtosis (solid) for stationary, Gaussian signals.

higher-order spectral moments of turbulent velocity and scalar fields is examined. Finally, the higher-order spectral moments of velocity and scalar fields are compared.

### 4.1. Algorithm testing and validation

As a first test, a time series of Gaussian white noise was generated using MATLAB and its spectral skewness and kurtosis were evaluated using the procedure described in § 2 to ensure that the algorithm did not falsely detect transients. The artificial signal consisted of 244 blocks of 4096 data points sampled at a frequency of 10 kHz. As recommended in § 2, several window lengths were evaluated to ensure that the results were consistent and not systematically forced to their Gaussian values by the central limit theorem. Figure 3 confirms that the algorithm returns the values of  $\Gamma(5/2)$  ( $\approx 1.33$ ) and 2 for the spectral skewness and kurtosis, respectively, of a stationary, Gaussian signal. It is therefore clear that the algorithm does not detect significant deviations from Gaussianity, regardless of the window length, such that any future observed deviations from Gaussianity will have originated from the intermittent behaviour of the turbulent signal.

To further test the algorithm's ability to detect transients and intermittent behaviour, another synthetic signal was constructed. It consisted of Gaussian white noise to which 11 short-lived transients of the form

$$x_{trans}(t) = A \cos(2\pi ft) e^{(\lambda(t-\tau)^2)}, \quad (4.1)$$

were superimposed, where  $f$  (the frequency of the transient) was varied from 990 to 1010 Hz and a unique temporal offset ( $\tau$ ) was randomly attributed to each transient. The discretised signal had a sampling frequency of 10 kHz and the magnitude of each transient was within 99.9 % of its maximum amplitude ( $A$ ) for 0.0074 s. Note that the purpose of

this synthetic signal was not to emulate turbulence, as the physics underlying the internal intermittency of turbulent flows are much more complicated. Rather, the synthetic signal is used to benchmark the ability of the higher-order spectral moments tools developed in § 2 to detect short, intermittent behaviour. The higher-order spectral moments of this signal are depicted in figure 4, in which one can observe a clear deviation from Gaussianity being detected by the algorithm around 1.0 kHz, which corresponds to the frequency of the added transients. Note that the skewness captures and locates the transients well, even though rare events in a given process may occur symmetrically (i.e. evenly in both tails of the distribution). The reason the spectral skewness is capable of detecting transients is that the tails of the distribution become combined when taking the magnitude of the Fourier modes. This concentrates the rare events to a single tail, which skews the distribution. Moreover, it is worth noting that the spectral kurtosis appears to be more sensitive to transients than the spectral skewness. This results from the higher statistical order of the spectral kurtosis. Figure 4 also clearly demonstrates that the magnitudes of the deviations from Gaussian behaviour decrease with increasing window length, further reinforcing the notion that higher-order spectral moments are dependent on the window length ( $N$ ). In this particular example, the effects of the window length are easily explained by comparing the length of the transients ( $n_{trans}$ ) to  $N$ . The number of sample points contained within each transient is equal to  $n_{trans} = f_s * t_{trans}$ , where  $f_s$  is the sampling frequency and  $t_{trans}$  is the duration of the transient. As previously mentioned, the transients in this example are approximately 0.0074 s long, yielding approximately 74 data points within each transient. Therefore, given the discussion in § 2.2, one could anticipate that a window length of  $N = 74$ , or slightly shorter, would maximise the higher-order spectral moments. The results presented in figure 4 support this argument, as the peak value of both spectral moments decreases as the length of the windows exceeds the length of the transients in the signal. Moreover, as the window length is shortened significantly below the length of the transients, the peak values of the higher-order spectral moments decrease as well. Nevertheless, the deviations from Gaussian behaviour are accurately situated and quantified in the frequency domain regardless of the window length, thus showing that the algorithm constructed in § 2 is capable of capturing rare, intermittent events in an otherwise Gaussian time series.

#### 4.2. Higher-order spectral moments of turbulent velocity fields

In this section, a systematic investigation of the evolution of the internal intermittency of turbulent velocity and passive-scalar fields in wavenumber space is undertaken by way of an analysis of the higher-order spectral moments of turbulent time series. To this end, figures 5 and 6 respectively plot the spectral skewness and spectral kurtosis of a turbulent velocity field at  $R_\lambda = 582$  as a function of normalised wavenumber  $\kappa_1 \eta$ , where  $\eta$  is the Kolmogorov length scale. Power spectra are also plotted in these figures to better identify the various ranges of the flow (e.g. the inertial subrange). Note that these results were obtained using STFT windows of length  $N = 625\eta$ . Although shorter windows would have maximised the higher-order spectral moments, longer windows include a larger range of frequencies, which is preferable at the initial stages of the analysis, given that they allow low-frequency deviations from Gaussianity to be captured. Results obtained using shorter windows that highlight the intermittency at higher frequencies are presented in subsequent sections.

It is worthwhile noting that some insight could have been gained from calculating the higher-order moments of differences in turbulent quantities (e.g. the kurtosis of velocity increments,  $K_{\Delta u}$ , ( $\Delta u = [u(x+r) - u(x)]$ )), as those are the real-space analogues of the

Intermittency and higher-order spectral moments

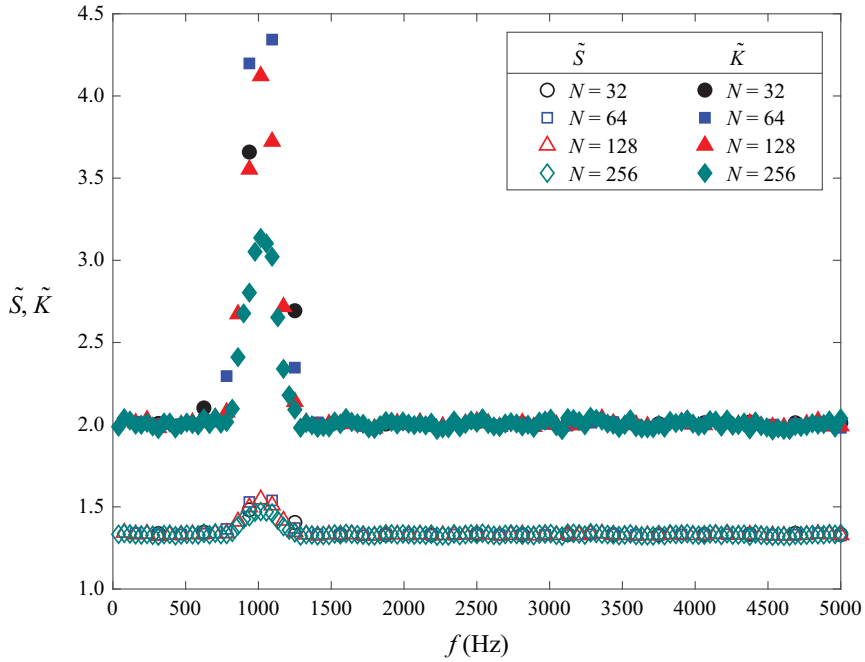


Figure 4. Spectral skewness (open symbols) and kurtosis (closed symbols) of Gaussian white noise with added transients evaluated using window lengths of 32 ( $\circ$ ,  $\bullet$  – black), 64 ( $\square$ ,  $\blacksquare$  – blue), 128 ( $\triangle$ ,  $\blacktriangle$  – red), 256 ( $\diamond$ ,  $\blacklozenge$  – green) samples.

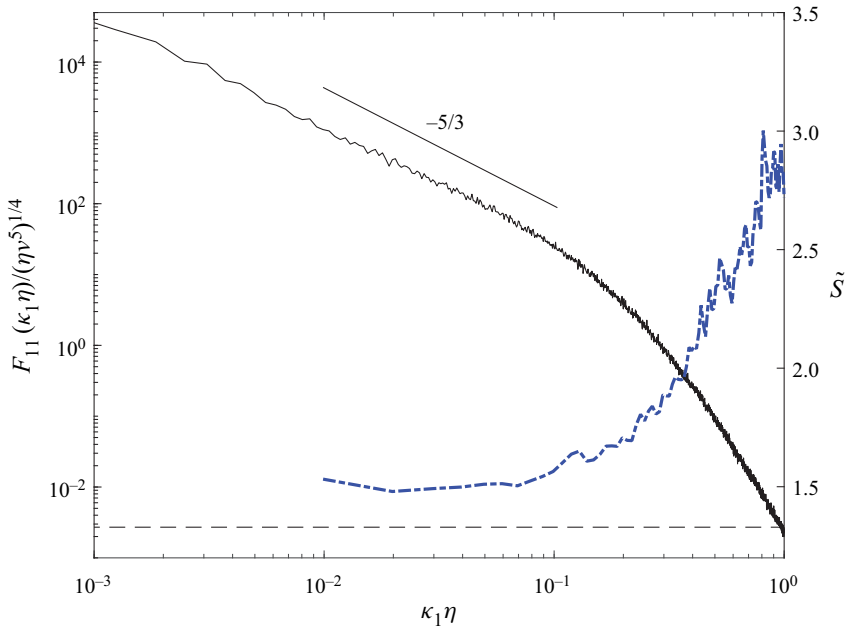


Figure 5. Longitudinal ( $u$ ) velocity spectrum (solid black line) and spectral skewness (dashed blue line) at  $R_\lambda = 582$ . Results are obtained using a window length  $625\eta$ .

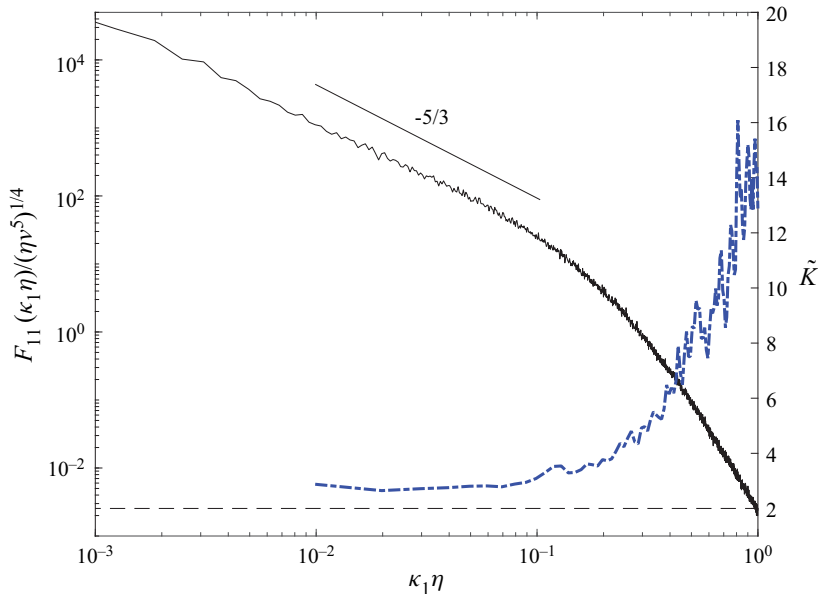


Figure 6. Longitudinal ( $u$ ) velocity spectrum (solid black line) and spectral kurtosis (dashed blue line) at  $R_\lambda = 582$ . Results are obtained using a window length  $625\eta$ .

spectral moments of equivalent statistical order. However, as noted in § 1, an important reason for undertaking the present analysis in the spectral domain is that structure functions (e.g.  $\Delta u(r)$ ) include contributions from all scales less than or equal to the scale  $r$  (see, for example, Meyer *et al.* 2018), whereas spectra quantify the contribution only at a specific scale ( $\kappa_1 \sim 1/r$ ).

The first important observation to be made regarding figures 5 and 6 is that both higher-order spectral moments asymptotically tend to their Gaussian values ( $\tilde{S} = \Gamma(5/2)$  and  $\tilde{K} = 2$ ) at large scales (low wavenumbers), thus confirming that little intermittency is present at the largest scales of the turbulence. Conversely, at high wavenumbers, one observes a sharp increase in both the spectral skewness and kurtosis, thus highlighting the highly intermittent behaviour of the turbulent velocity field at dissipative scales. Note that these observations are consistent with figure 6 of Brun & Pumir (2001) and figure 1(a) of Chevillard *et al.* (2005), who observed a plateau at large scales and increased intermittent activity in the dissipation range using fourth-order spectral moments applied to time series of velocity fields from numerical and experimental data, respectively. Chevillard *et al.* (2005) also calculated the fourth-order spectral moment of an intermittent synthetic signal, as a proxy for turbulence at high Reynolds number (with no dissipation range), which yielded a similar plateau. They found that the magnitude of the plateau evolved as a power law of the width of the windowing function (arguing that longer windows were associated with larger scales and therefore lower values of the fourth-order spectral moments). However, our prior analysis demonstrated that longer window lengths are associated with lower values of the higher-order spectral moments due to consequences of the central limit theorem.

These preliminary observations clearly demonstrate that both higher-order spectral moments studied herein are able to detect deviations from Gaussianity and thus internal intermittency. Moreover, the insight provided by the higher-order spectral moments



compared with time-domain statistical moments is also readily demonstrated. The calculation of higher-order moments in short spectral bands allows (i) deviations from Gaussian behaviour to be located in wavenumber space, and (ii) an evaluation of the relative magnitude of the deviations from Gaussianity at each scale. The deviation from Gaussianity extends to the high-wavenumber end of the inertial subrange. This will be further discussed when short-window results are introduced, as these provide an even better depiction of inertial subrange intermittency. These features of higher-order spectral moments will be used to study the internal intermittency of turbulent velocity and passive-scalar fields in the following subsections.

#### 4.3. Reynolds-number dependence of higher-order spectral moments

Figure 7 depicts the evolution of the spectral skewness and kurtosis of the longitudinal velocity fluctuations ( $u$ ), transverse velocity fluctuations ( $v$ ) and scalar fluctuation ( $\theta$ ) in grid-generated turbulence at five different Reynolds numbers in the range  $35 \leq R_\lambda \leq 582$ . Note that these results were generated using a shorter window length of  $N = 150\eta$ , thereby highlighting transient behaviour at the smaller-scale end of the inertial subrange and in the dissipation range. The results depict a very clear dependence on Reynolds number, even at  $R_\lambda < 100$  which was previously observed to be the threshold for the hydrodynamic (inertial-range) intermittency exponent ( $\mu$ ) to depart from zero (Mydlarski & Warhaft 1998). However, Mydlarski & Warhaft (1998) observed the scalar field intermittency exponent ( $\mu_\theta$ ) to be non-zero at even the lowest of Reynolds/Péclet numbers. A significant increase in non-Gaussian behaviour is exhibited by all spectral moments as the Reynolds number is increased. Note that this increase in magnitude of the spectral moments occurs at all scales covered by the chosen window length, and applies to all turbulent fields under study (i.e.  $u$ ,  $v$  and  $\theta$ ). Moreover, note that the scale at which a strong and rapid departure from Gaussianity is observed shifts towards larger scales as the Reynolds number increased.

One can further explore the Reynolds-number dependence of internal intermittency by investigating the evolution of the magnitude of the higher-order spectral moments evaluated at a particular length scale. A length scale of interest is the wavenumber at which the dissipations of turbulent kinetic energy and turbulent scalar variance spectra peak, which is observed to occur around  $\kappa_1\eta = 0.2$  for the velocity and scalar fields, although the exact location of this peak is Reynolds-number dependent (Tennekes & Lumley 1972; Mydlarski & Warhaft 1996, 1998). The value of the spectral skewness and kurtosis at a normalised wavenumber of  $\kappa_1\eta = 0.2$  is plotted in figure 8 as a function of  $R_\lambda$  over the range  $35 \leq R_\lambda \leq 731$ . Note that the higher-order spectral moments shown in figure 8 were obtained using the same window length as that used in figure 7 ( $N = 150\eta$ ). Although some scatter is observed, the plots confirm the increase in both the spectral skewness and spectral kurtosis (and therefore in internal intermittency) at a fixed wavenumber as  $R_\lambda$  is increased. Moreover, considering each higher-order spectral moment individually, note that the power law fits are consistent for the longitudinal and transverse velocity and passive-scalar fields, with  $\tilde{S}(\kappa_1\eta = 0.2)$  increasing as  $R_\lambda^{0.1}$  and  $\tilde{K}(\kappa_1\eta = 0.2)$  increasing as  $R_\lambda^{0.3}$  for the spectral kurtosis. The evolution of the spectral skewness and kurtosis is further explored in figure 9, in which the Reynolds-number dependence of both spectral moments evaluated at  $\kappa_1\eta = 0.8$  is investigated. Note that the chosen length scale of  $\kappa_1\eta = 0.8$  is believed to offer a good representation of the intermittent behaviour of the flow as the Kolmogorov length scale is approached ( $\kappa_1\eta \rightarrow 1$ ), while staying sufficiently far away from the Kolmogorov length scale where errors due to low-pass filter roll-off and probe

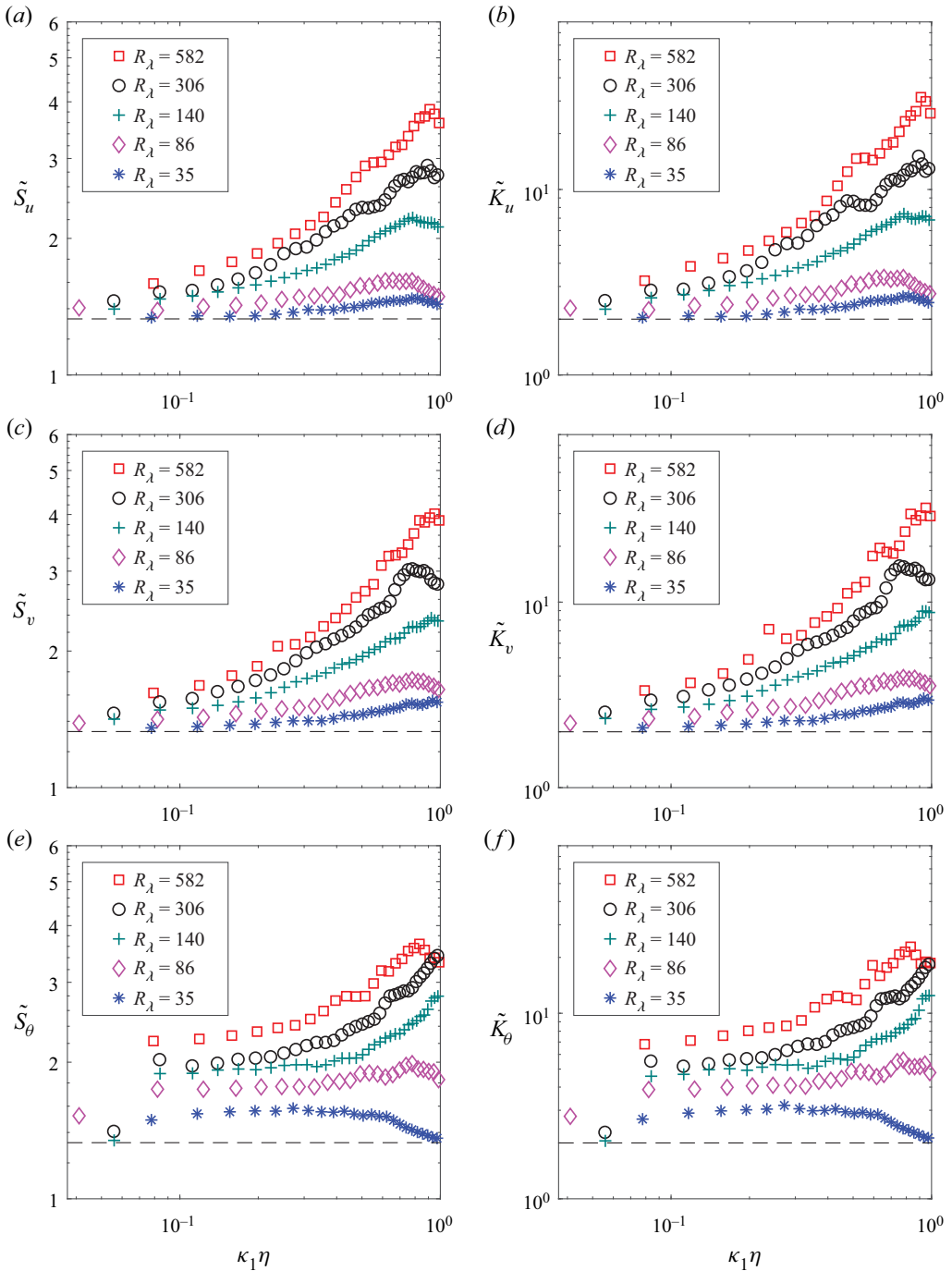


Figure 7. Spectral skewness (a,c,e) and kurtosis (b,d,f) of the longitudinal velocity fluctuations  $u$  (a,b), the transverse velocity fluctuations  $v$  (c,d) and the scalar (temperature) fluctuations  $\theta$  (e,f) at  $R_\lambda = 35$  (\*, blue),  $R_\lambda = 86$  ( $\diamond$ , magenta),  $R_\lambda = 140$  (+, green),  $R_\lambda = 306$  ( $\circ$ , black) and  $R_\lambda = 582$  ( $\square$ , red). Results are obtained using a window length  $N = 150\eta$ .

Intermittency and higher-order spectral moments

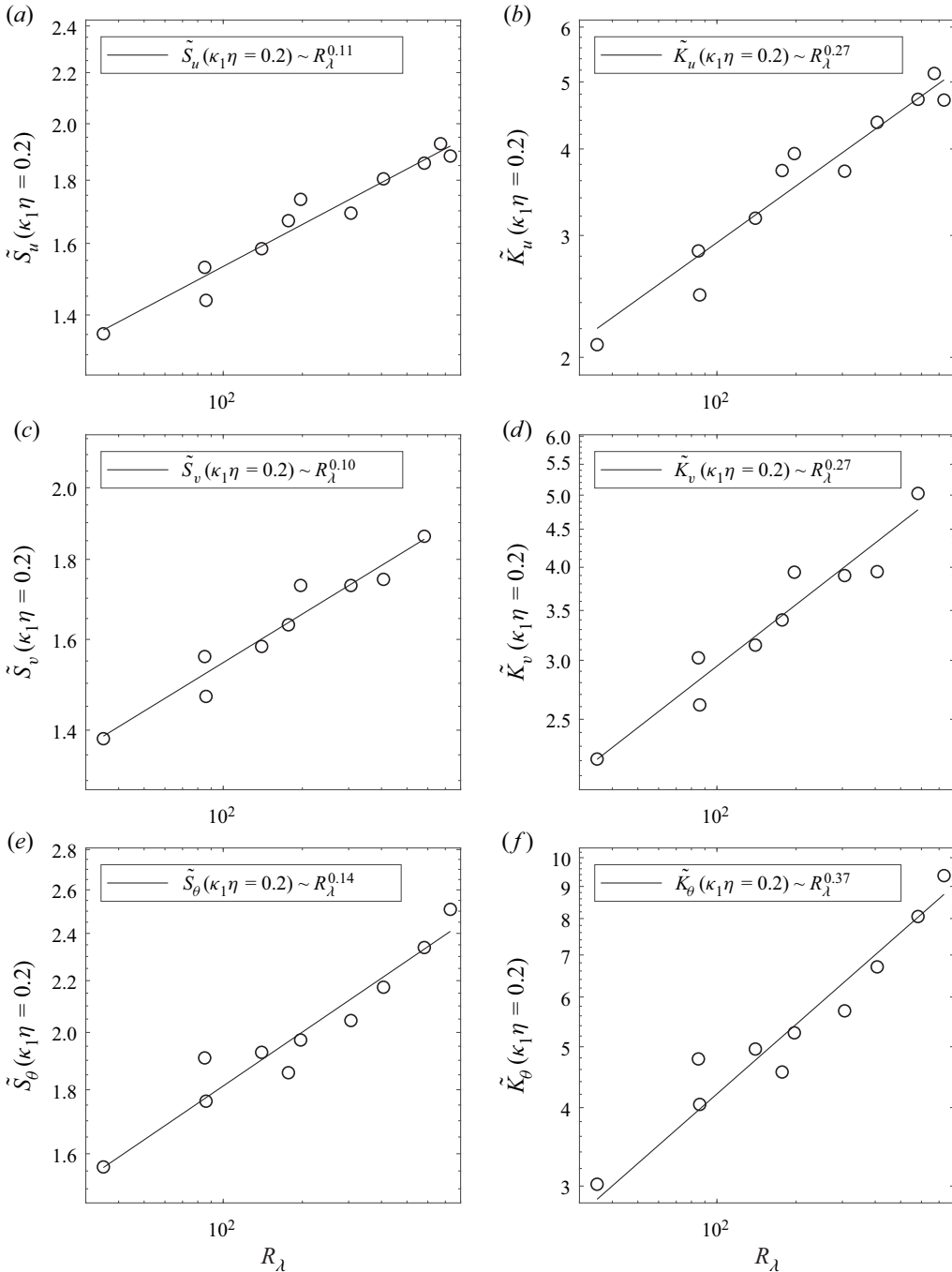


Figure 8. Reynolds-number dependence of the spectral skewness (a,c,e) and kurtosis (b,d,f) of the longitudinal velocity fluctuations  $u$  (a,b), the transverse velocity fluctuations  $v$  (c,d) and the passive-scalar (temperature) fluctuations  $\theta$  (e,f) evaluated at  $\kappa_1\eta = 0.2$ . The solid black lines represent the best fit power laws. Results are obtained using a window length  $N = 150\eta$ .

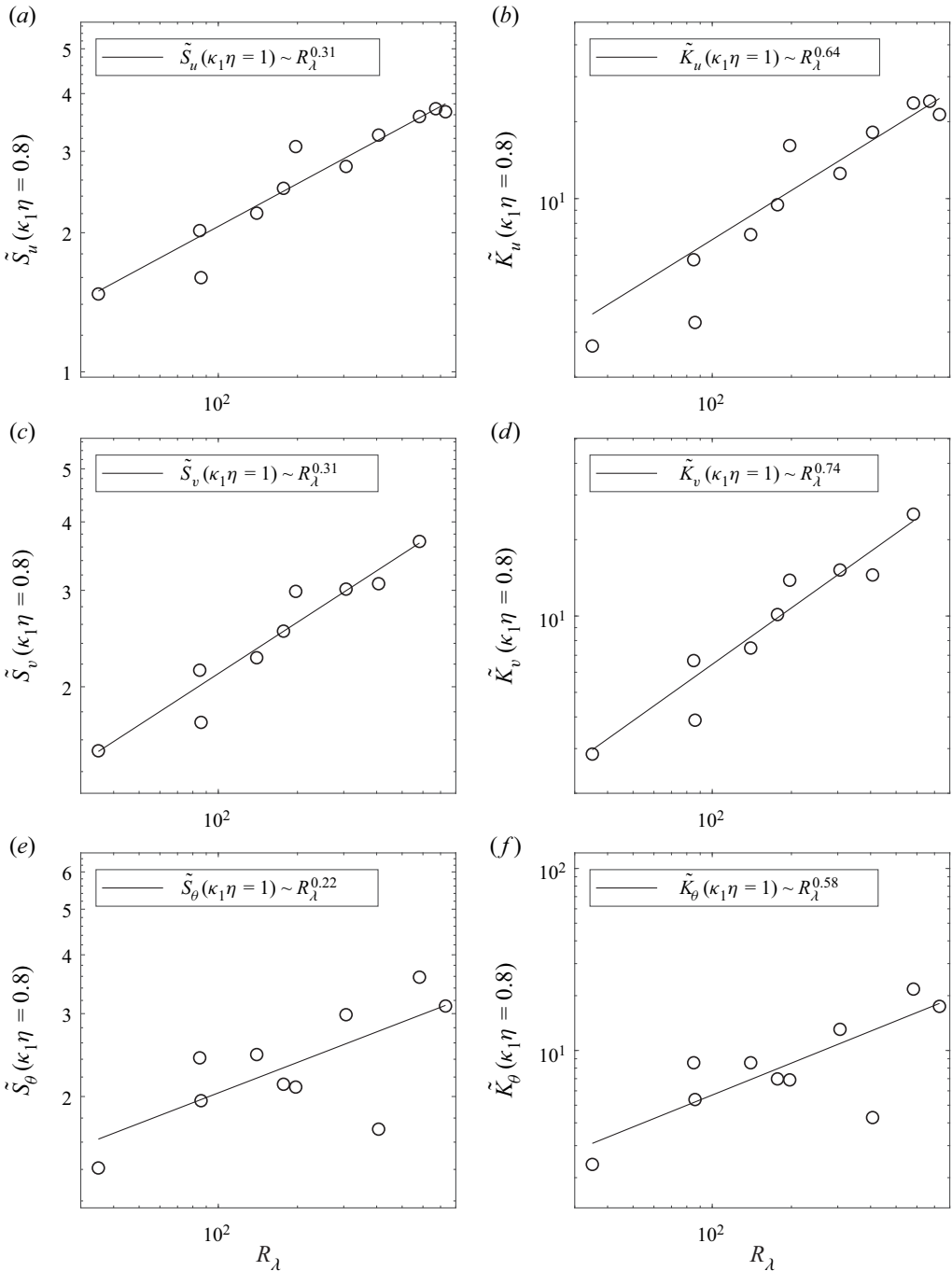


Figure 9. Reynolds-number dependence of the spectral skewness (a,c,e) and kurtosis (b,d,f) of the longitudinal velocity fluctuations  $u$  (a,b), the transverse velocity fluctuations  $v$  (c,d) and the passive-scalar (temperature) fluctuations  $\theta$  (e,f) evaluated at  $\kappa_1\eta = 0.8$ . The solid black lines represent the best fit power laws. Results are obtained using a window length  $N = 150\eta$ .

frequency resolution (especially with cold-wire thermometers) may occur (Kuo & Corrsin 1971). As was the case at  $\kappa_1\eta = 0.2$ , the Reynolds-number dependence of the spectral skewness and kurtosis at  $\kappa_1\eta = 0.8$  is consistent with a power law increase, although a stronger dependence on Reynolds number is observed at this smaller length scale. These changes in power law exponents with  $\kappa_1\eta$  highlight the wavenumber dependence of the evolution of the higher-order spectral moments with  $R_\lambda$ .

To place these results in the context of prior studies of internal intermittency, it is of benefit to compare the present work with prior investigations of the dependence of internal intermittency on Reynolds number, which was historically investigated using the kurtosis of derivatives of turbulence quantities (e.g.  $K_{\partial u/\partial x}$ ,  $K_{\partial\theta/\partial x}$ ) as measures of the degree of intermittency in turbulent flows (see Van Atta & Antonia 1980; Sreenivasan & Antonia 1997). Studies have shown that  $K_{\partial u/\partial x}$  and  $K_{\partial\theta/\partial x}$  are strongly dependent on Reynolds number, with  $K_{\partial u/\partial x}$  increasing as  $\sim R_\lambda^{3/8}$  (Van Atta & Antonia 1980), which is consistent with the observations of the spectral kurtosis evaluated at  $\kappa_1\eta = 0.2$  (figure 8). As previously noted, the Reynolds-number dependence of the spectral skewness and kurtosis was specifically evaluated at  $\kappa_1\eta = 0.2$  because this normalised wavenumber ( $\kappa_1\eta = 0.2$ ) approximately corresponds to that of the peak of the dissipation spectrum (Tennekes & Lumley 1972). Given that dissipation spectra can also be interpreted as the spectra of the derivative, studying the higher-order spectral moments at  $\kappa_1\eta = 0.2$  evaluates them at the wavenumber at which the derivative has its maximum contribution, thus explaining the agreement between the observed trends ( $\sim R_\lambda^{0.3}$ ) and those obtained by examining the Reynolds-number dependencies of  $K_{\partial u/\partial x}$  and  $K_{\partial\theta/\partial x}$  ( $\sim R_\lambda^{3/8}$ ). However, it bears reiterating that the present results have demonstrated that the Reynolds-number dependence of internal intermittency depends upon wavenumber, as demonstrated by the scale-by-scale analysis achieved by way of higher-order spectral moments.

In addition to the above results, another approach was also employed in an attempt to investigate any possible Reynolds-number dependencies associated with the use of a window length of fixed multiples of  $\eta$  as the Reynolds number changes. To this end, the data were reanalysed using a window length ( $N$ ) that evolved with Reynolds number in such a way the window length was equal to the separation that corresponds to the mid-point of the inertial subrange for each flow. To determine the required window length for this approach, we followed the methodology employed in Mydlarski & Warhaft (1996, 1998), who developed an approach for the calculation of conditional statistics of inertial-range velocity and scalar increments (e.g.  $\Delta u(r)$ ) as the Reynolds/Péclet number increased. This approach is depicted in figure 23 of Mydlarski & Warhaft (1996). These authors chose a single value of  $r$  (denoted as  $r_a$  in Mydlarski & Warhaft 1996) that corresponded to the wavenumber  $\kappa_1$  ( $r = 2\pi/\kappa_1$ ) that lay half-way between the beginning and end of the scaling range for each spectrum. Thus as the scaling range dilated with Reynolds number,  $r_a$  remained in the same relative position within the inertial subrange. Using this approach, the window lengths varied from one case to the next, but always remained in the same relative position on the spectrum, independent of Reynolds number.

Figure 10 plots the spectral skewness and kurtosis of the  $u$ ,  $v$  and  $\theta$  fields using this approach for different Reynolds numbers for window lengths  $N$  equal to  $r_a$ . Although there are differences in the results when this new methodology is employed to specify the window widths, the overall (quantitative and qualitative) results and trends in figures 7 and 10 remain quite similar, thus justifying the robustness of the analysis herein and confirming the relative insensitivity of the effect of window width when the Reynolds number is varied.

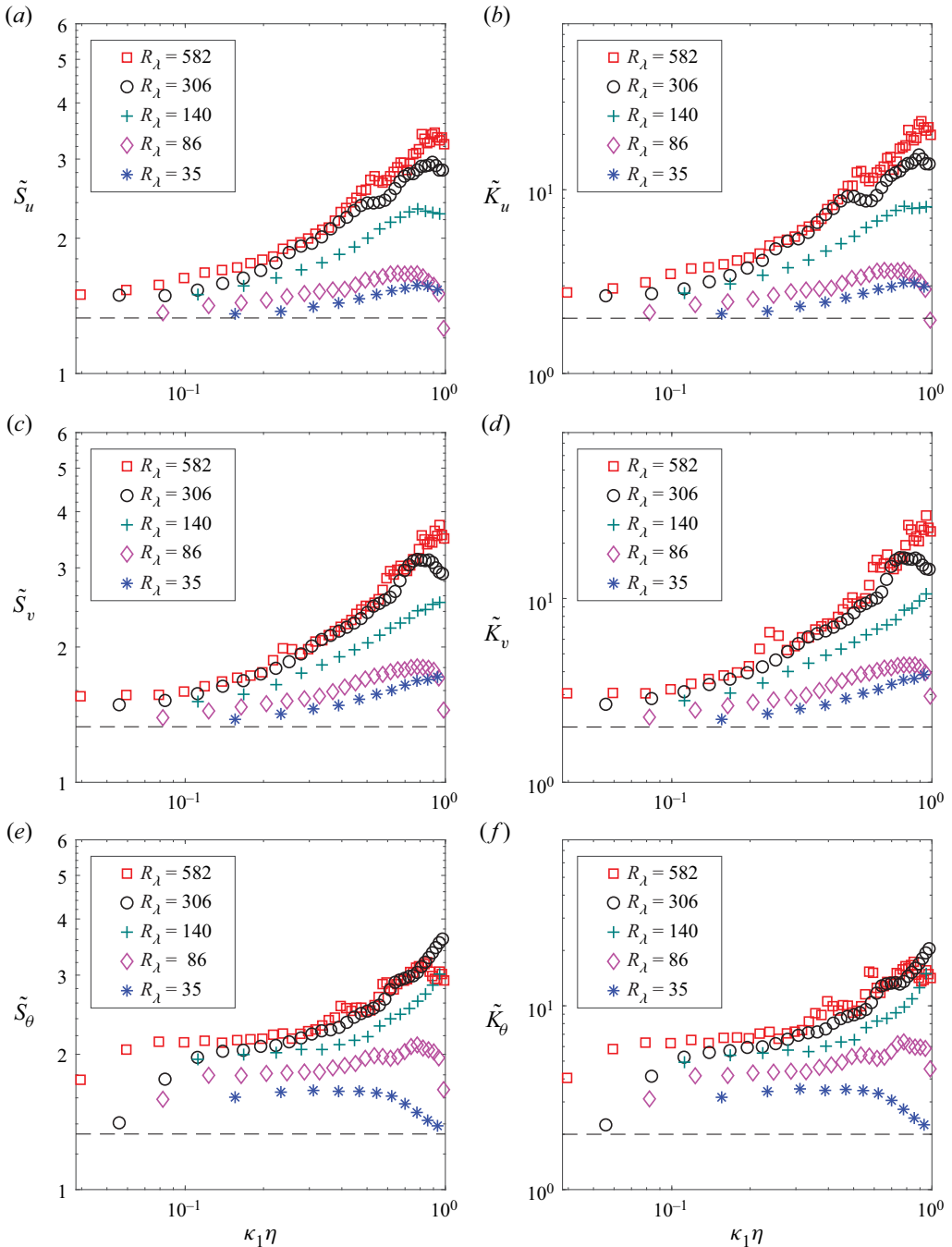


Figure 10. Spectral skewness (*a,c,e*) and kurtosis (*b,d,f*) of the longitudinal velocity fluctuations  $u$  (*a,b*), the transverse velocity fluctuations  $v$  (*c,d*) and the scalar (temperature) fluctuations  $\theta$  (*e,f*) at  $R_\lambda = 35$  (\*, blue),  $R_\lambda = 86$  ( $\diamond$ , magenta),  $R_\lambda = 140$  (+, green),  $R_\lambda = 306$  ( $\circ$ , black) and  $R_\lambda = 582$  ( $\square$ , red). Results are obtained using window lengths corresponding to the midpoint of the inertial subrange.

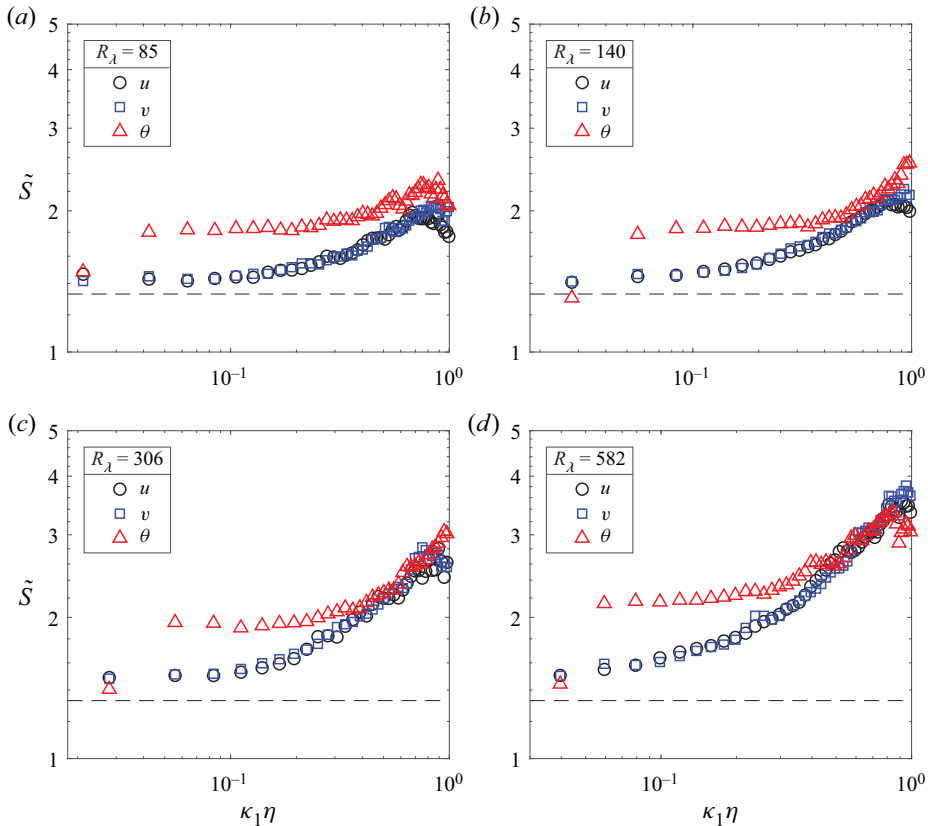


Figure 11. Spectral skewness of the longitudinal velocity fluctuations  $u$  ( $\circ$ , black), transverse velocity fluctuations  $v$  ( $\square$ , blue) and scalar (temperature) fluctuations  $\theta$  ( $\triangle$ , red) at (a)  $R_\lambda = 85$ , (b)  $R_\lambda = 140$ , (c)  $R_\lambda = 306$  and (d)  $R_\lambda = 582$ . Results are obtained using a window length  $N = 220\eta$ .

#### 4.4. Higher-order spectral moments of turbulent scalar fields

Given the different nature of scalar fields (Pumir *et al.* 1991; Holzer & Siggia 1994; Warhaft 2000), it is of particular interest to study the relative levels of intermittency of both velocity and passive-scalar fields. To this end, a preliminary analysis (not shown) concluded that a window length of  $N = 220\eta$  captured the signal transients while also fully capturing frequencies in the dissipation range and most of the inertial–convective subrange.

Plots of the spectral skewness and kurtosis of  $u$ ,  $v$  and  $\theta$  are given in figures 11 and 12, respectively. The overall behaviour of all higher-order spectral moments is similar for all three quantities. More specifically, the curves all show a significant departure from Gaussian behaviour at small scales, and both the spectral skewness and kurtosis exhibit a higher degree of internal intermittency in the inertial–convective subrange for passive-scalar fields (compared with the longitudinal and transverse velocity fields, which are both very similar in magnitude in the inertial subrange). Note that these results are consistent with those of Mydlarski & Warhaft (1998), who used the velocity and scalar intermittency exponent to show that scalar fields were more intermittent in the inertial subrange and that their level of intermittent activity increased with Reynolds number.

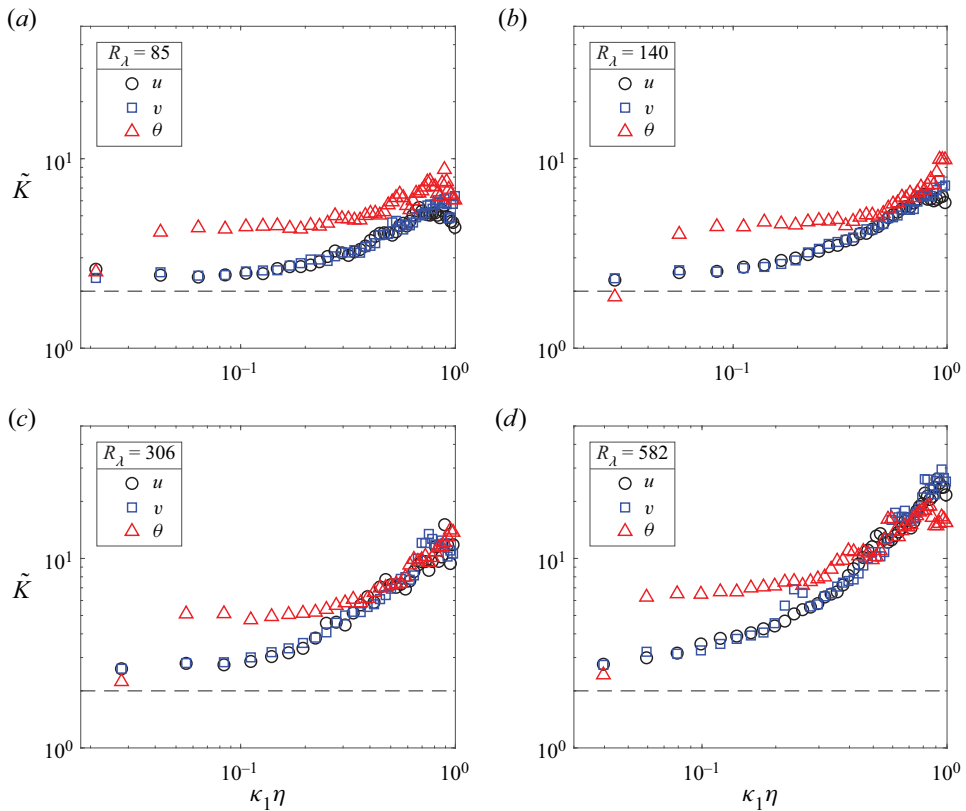


Figure 12. Spectral kurtosis of the longitudinal velocity fluctuations  $u$  ( $\circ$ , black), transverse velocity fluctuations  $v$  ( $\square$ , blue) and scalar (temperature) fluctuations  $\theta$  ( $\triangle$ , red) at (a)  $R_\lambda = 85$ , (b)  $R_\lambda = 140$ , (c)  $R_\lambda = 306$  and (d)  $R_\lambda = 582$ . Results are obtained using a window length  $N = 220\eta$ .

Moreover, they also showed that the level of inertial range intermittency of passive-scalar fields remains higher than that of velocity fields at all Reynolds numbers.

The results presented in figures 11 and 12 show that the spectral skewness and spectral kurtosis of the scalar fluctuations remain at a higher level at small scales (high wavenumbers) when compared with the longitudinal and transverse velocity statistics for the two lower  $R_\lambda$  cases shown in figures 11 and 12. However, the spectral skewness and spectral kurtosis of the longitudinal and transverse velocity fluctuations undergo a rapid increase in the dissipation range and reach levels similar to that of the passive-scalar field as  $\kappa_1\eta \rightarrow 1$  for the two higher  $R_\lambda$  cases. This suggests that passive-scalar fields are more intermittent in the inertial–convective subrange and in part of the dissipation range, but the degree of intermittency of the streamwise and transverse velocity fields becomes similar to that of the scalar field as the Kolmogorov length scale is approached at high Reynolds numbers. This is consistent with the remarks made in § 4.3 regarding the wavenumber dependence of the Reynolds-number evolution of higher-order spectral moments. The plots of figure 9 showed that dependence of higher-order spectral moments on Reynolds number was stronger for the velocity field than the passive-scalar field at high wavenumbers. This is the reason figures 11 and 12 show that the higher-order spectral moments of both components of the velocity field reach levels similar to those of the passive-scalar field at high wavenumbers for the two highest  $R_\lambda$  cases.



## 5. Summary and conclusions

Higher-order spectral moments have been used to investigate internal intermittency in grid-generated turbulent velocity and passive scalar fields. In this study, an overview of the theory behind the third- and fourth-order spectral moments was first presented. Then, a STFT-based estimator was used to develop an algorithm capable of calculating higher-order spectral moments. The estimator was validated using Gaussian and non-Gaussian test signals, and the dependence of the estimator on window length was investigated. It was demonstrated that higher-order spectral moments can be used to situate intermittency in wavenumber space and compare the relative levels of intermittency at different scales. Higher-order spectral moments of turbulent flows were shown to exhibit repeatable behaviours, asymptotically moving to Gaussian values at large scales and departing from Gaussian behaviour in the inertial subrange, reaching their maximum values at the smallest scales of the dissipation range. Additionally, it was demonstrated that higher-order spectral moments are Reynolds-number dependent. The spectral kurtoses of the longitudinal and transverse velocity fields at  $\kappa_1\eta = 0.2$  were found to increase as  $\tilde{K}_{u\alpha}(\kappa_1\eta = 0.2) \sim R_\lambda^{0.3}$  over the range of Reynolds numbers studied herein, which is consistent with the behaviour of the overall kurtosis of velocity derivatives observed by Van Atta & Antonia (1980). Moreover, the Reynolds-number dependence of the intensity of internal intermittency was shown to depend on wavenumber by way of the present approach.

The magnitude and wavenumber dependence of the internal intermittency of passive-scalar fields was compared with that of velocity fields with the spectral skewness and kurtosis revealing that the level of intermittency of passive-scalar fluctuations is higher in the inertial subrange and part of the dissipation range when compared with those of the longitudinal and transverse velocity fluctuations. However, for the higher  $R_\lambda$  cases and as  $\kappa_1\eta \rightarrow 1$ , the levels of intermittency of the longitudinal and transverse velocity fluctuations were seen to increase and eventually become similar to those of the passive-scalar field.

The results herein suggest that our knowledge of internal intermittency can be expanded by way of higher-order spectral moments. In the present work, the latter provided an insightful means of investigating the Reynolds-number dependence of intermittency and comparing the intermittent behaviour of velocity and passive-scalar fields. Future work shall be aimed at comparing the wavenumber dependence and levels of intermittency between different classes of flows. It is hoped that higher-order spectral moments can be used to investigate additional turbulence phenomena, such as the evolution of the coherent structures in wall-bounded flows, or other intermittent phenomena.

**Acknowledgements.** The authors acknowledge the reviewers for their constructive comments, which improved this work.

**Funding.** Support for this work was graciously provided by the Natural Sciences and Engineering Council of Canada (Grant number RGPIN-2018-05848), as well as the United States Department of Energy (Basic Energy Sciences). The experiments were undertaken at Cornell University. Funding for S.L. was provided by the Natural Sciences and Engineering Council of Canada (Canada Graduate Scholarships – Master’s program) and the Fonds de recherche du Québec – Nature et technologies (Master’s research scholarships).

**Declaration of interests.** The authors report no conflict of interest.

**Author ORCIDs.**

 L. Mydlarski <https://orcid.org/0000-0002-5284-3742>.

## REFERENCES

- ANSELMET, F., GAGNE, Y., HOPFINGER, E.J. & ANTONIA, R.A. 1984 High-order velocity structure functions in turbulent shear flows. *J. Fluid Mech.* **140**, 63–89.
- ANTONI, J. 2006 The spectral kurtosis: a useful tool for characterising non-stationary signals. *Mech. Syst. Signal Pr.* **20** (2), 282–307.
- ANTONI, J. 2007 Fast computation of the kurtogram for the detection of transient faults. *Mech. Syst. Signal Pr.* **21** (1), 108–124.
- ANTONI, J. & RANDALL, R.B. 2006 The spectral kurtosis: application to the vibratory surveillance and diagnostics of rotating machines. *Mech. Syst. Signal Pr.* **20** (2), 308–331.
- BATCHELOR, G.K. & TOWNSEND, A.A. 1949 The nature of turbulent motion at large wave-numbers. *P. R. Soc. Lond. A Mat.* **199** (1057), 238–255.
- BOS, W.J.T., LIECHTENSTEIN, L. & SCHNEIDER, K. 2007 Small-scale intermittency in anisotropic turbulence. *Phys. Rev. E* **76** (4), 046310.
- BRUN, C. & PUMIR, A. 2001 Statistics of fourier modes in a turbulent flow. *Phys. Rev. E* **63** (5), 056313.
- CHEVILLARD, L., MAZELLIER, N., POULAIN, C., GAGNE, Y. & BAUDET, C. 2005 Statistics of Fourier modes of velocity and vorticity in turbulent flows: intermittency and long-range correlations. *Phys. Rev. Lett.* **95** (20), 200203.
- CORRSIN, S. 1951 On the spectrum of isotropic temperature fluctuations in an isotropic turbulence. *J. Appl. Phys.* **22** (4), 469–473.
- DJENIDI, L., ANTONIA, R.A. & TANG, S.L. 2019 Scale invariance in finite Reynolds number homogeneous isotropic turbulence. *J. Fluid Mech.* **864**, 244–272.
- DWYER, R.F. 1983 A technique for improving detection and estimation of signals contaminated by under ice noise. *J. Acoust. Soc. Am.* **74** (1), 124–130.
- FARGE, M. 1992 Wavelet transforms and their applications to turbulence. *Annu. Rev. Fluid Mech.* **24** (1), 395–458.
- FORBES, C., EVANS, M., HASTINGS, N. & PEACOCK, B. 2011 *Statistical Distributions*. John Wiley & Sons.
- FRISCH, U. 1995 *Turbulence: The Legacy of A.N. Kolmogorov*. Cambridge University Press.
- HOLZER, M. & SIGGIA, E.D. 1994 Turbulent mixing of a passive scalar. *Phys. Fluids* **6** (5), 1820–1837.
- HU, Y., BAO, W., TU, X., LI, F. & LI, K. 2019 An adaptive spectral kurtosis method and its application to fault detection of rolling element bearings. *IEEE Trans. Instrum. Meas.* **69** (3), 739–750.
- KENNEDY, D.A. & CORRSIN, S. 1961 Spectral flatness factor and ‘intermittency’ in turbulence and in non-linear noise. *J. Fluid Mech.* **10** (3), 366–370.
- KOLMOGOROV, A.N. 1941a Dissipation of energy in the locally isotropic turbulence. *Dokl. Akad. Nauk. SSSR* **32**, 16–18.
- KOLMOGOROV, A.N. 1941b The local structure of turbulence in incompressible viscous fluid for very large Reynolds numbers. *Dokl. Akad. Nauk. SSSR* **30**, 301–305.
- KRAICHNAN, R.H. 1994 Anomalous scaling of a randomly advected passive scalar. *Phys. Rev. Lett.* **72** (7), 1016–1019.
- KUO, A.Y. & CORRSIN, S. 1971 Experiments on internal intermittency and fine-structure distribution functions in fully turbulent fluid. *J. Fluid Mech.* **50** (2), 285–319.
- LANDAU, L.D. 1944 On the problem of turbulence. *Dokl. Akad. Nauk. USSR* **44**, 311.
- LEITE, V.C., BORGES DA SILVA, J.G., BORGES DA SILVA, L.E., VELOSO, G.F.C., LAMBERT-TORRES, G., BONALDI, E.L. & DE OLIVEIRA, L.E.L. 2016 Experimental bearing fault detection, identification, and prognosis through spectral kurtosis and envelope spectral analysis. *Electr. Pow. Compo. Sys.* **44** (18), 2121–2132.
- LEPORE, J. & MYDLARSKI, L. 2012 Finite-Péclet-number effects on the scaling exponents of high-order passive scalar structure functions. *J. Fluid Mech.* **713**, 453–481.
- MAKITA, H. 1991 Realization of a large-scale turbulence field in a small wind tunnel. *Fluid Dyn. Res.* **8** (1–4), 53–64.
- MENEVEAU, C. 1991 Analysis of turbulence in the orthonormal wavelet representation. *J. Fluid Mech.* **232**, 469–520.
- MEYER, C.R., MYDLARSKI, L. & DANAILA, L. 2018 Statistics of incremental averages of passive scalar fluctuations. *Phys. Rev. Fluids* **3** (9), 094603.
- MILLIOZ, F., HUILLERY, J. & MARTIN, N. 2006 Short time Fourier transform probability distribution for time-frequency segmentation. *Intl Conf. Acoust. Speech* **3**, 448–451.
- MYDLARSKI, L. 2017 A turbulent quarter century of active grids: from Makita (1991) to the present. *Fluid Dyn. Res.* **49** (6), 061401.
- MYDLARSKI, L. & WARHAFT, Z. 1996 On the onset of high-Reynolds-number grid-generated wind tunnel turbulence. *J. Fluid Mech.* **320**, 331–368.

## *Intermittency and higher-order spectral moments*

- MYDLARSKI, L. & WARHAFT, Z. 1998 Passive scalar statistics in high-Péclet-number grid turbulence. *J. Fluid Mech.* **358**, 135–175.
- NELKIN, M. 1990 Multifractal scaling of velocity derivatives in turbulence. *Phys. Rev. A* **42** (12), 7226.
- OBOUKHOV, A.M. 1949 Structure of the temperature field in turbulent flows. *Akad. Nauk. SSSR* **13**, 58–69.
- PAGNAN, S., OTTONELLO, C. & TACCONI, G. 1994 Filtering of randomly occurring signals by kurtosis in the frequency domain. In *International Journal of Pattern Recognition*, pp. 131–133. IEEE.
- PELIGRAD, M. & WU, W.B. 2010 Central limit theorem for Fourier transforms of stationary processes. *Ann. Probab.* **38** (5), 2009–2022.
- PRESS, W.H., WILLIAM, H., TEUKOLSKY, S.A., SAUL, A., VETTERLING, W.T. & FLANNERY, B.P. 2007 *Numerical Recipes 3rd edition: The Art of Scientific Computing*. Cambridge University Press.
- PUMIR, A., SHRAIMAN, B.I. & SIGGIA, E.D. 1991 Exponential tails and random advection. *Phys. Rev. Lett.* **66** (23), 2984.
- SREENIVASAN, K.R. & ANTONIA, R.A. 1997 The phenomenology of small-scale turbulence. *Annu. Rev. Fluid Mech.* **29** (1), 435–472.
- TENNEKES, H. & LUMLEY, J.L. 1972 *A First Course in Turbulence*. MIT Press.
- VAN ATTA, C.W. & ANTONIA, R.A. 1980 Reynolds number dependence of skewness and flatness factors of turbulent velocity derivatives. *Phys. Fluids* **23** (2), 252–257.
- WARHAFT, Z. 2000 Passive scalars in turbulent flows. *Annu. Rev. Fluid Mech.* **32** (1), 203–240.
- WELCH, P. 1967 The use of fast Fourier transform for the estimation of power spectra: a method based on time averaging over short, modified periodograms. *IEEE Trans. Acoust. Speech* **15** (2), 70–73.
- WYNGAARD, J.C. 1967 An experimental investigation of the small-scale structure of turbulence in a curved mixing layer, PhD thesis, The Pennsylvania State University.
- YAGLOM, A.M. 1949 On the local structure of a temperature field in a turbulent flow. *Dokl. Akad. Nauk. SSSR* **69**, 743–746.